# Mn-Doped CeO$_2$: DFT+U Study of a Catalyst for Oxidation Reactions

Delfina García Pintos,[†] Alfredo Juan,[‡] and Beatriz Irigoyen*[,†]

[†]Departamento de Ingeniería Química, Facultad de Ingeniería, Universidad de Buenos Aires, Pabellón de Industrias, Ciudad Universitaria, (C1428EGA) Ciudad Autónoma de Buenos Aires, Argentina
[‡]IFISUR-UNS-CONICET, Avda. Alem 1253, (B8000CPB) Bahía Blanca, Argentina

Ⓢ Supporting Information

ABSTRACT: In this work, we performed DFT+U periodic calculations to study the geometric and electronic properties of 12.5% Mn-doped CeO$_2$ solid solution. The doping with Mn allowed some Mn^{2+} cations to substitute Ce^{4+} ions into the CeO$_2$ lattice and thus drove the formation of a stable O-deficient bulk fluorite-type structure. The Mn-doped CeO$_2$(1 1 1) surface, generated upon the cleavage of the O-deficient bulk, exhibits Mn cations in a (3+) oxidation state. Spin-polarized energy calculations and charge analysis also evidenced the effect of Mn-dopant in facilitating the creation of surface oxygen vacancies; which reflected in extended surface and subsurface ions relaxation and reduction of Mn atoms located on surface and inner cationic layers. Concerning the oxidation state of Ce, it remained unaltered as Ce^{4+} when an O atom was removed from the topmost anionic layer of the surface system. Reduction of a Ce^{4+} cation to Ce^{3+} was evidenced after the creation of a second surface O-vacancy. Our results indicate facilitated surface oxygen release, Mn^{3+}/Mn^{2+} redox couples formation, and promoted anionic mobility and can help to better understand the effect of Mn in enhancing Mn-doped CeO$_2$ catalytic performance in oxidation reactions.
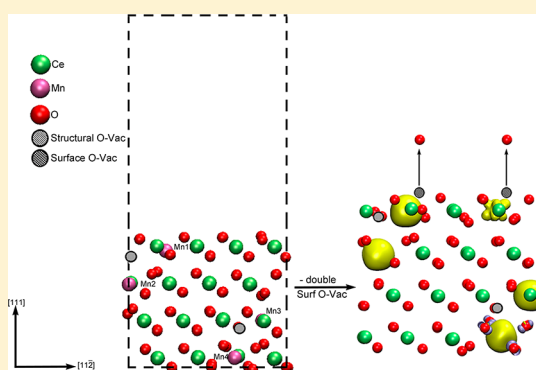
1. INTRODUCTION

Cerium-oxide-based materials are extensively used as catalysts due to their ability to participate efficiently in oxidation reactions and many other O-consuming processes.[1−3] The mechanism to release and store oxygen under oxidizing and reducing conditions has been related to their redox properties as they undergo constant rapid reduction/oxidation reversible cycles during the reaction process.[4,5]

Undoped CeO$_2$ presents good oxygen-storage capacity but is still insufficient for attaining the high performance required for industrial catalysts and also poor thermal resistance and stability under high-temperature operation conditions. The performance of CeO$_2$-based materials, mainly related to the presence of Ce^{4+}/Ce^{3+} couples, reduction facility, and oxygen mobility, could be improved by the addition of transition, alkaline earth, or rare-earth metals.[1,6] The doping of CeO$_2$ with transition metals, which usually exhibit several oxidation states and better redox properties than rare-earth metals, results in composite oxides with promoted oxygen storage capacity (OSC).[7] These mixed oxides show improved redox properties, mainly by the facilitated surface and bulk O-vacancies formation due to transition-metal incorporation into CeO$_2$ structure.[8]

In particular, Mn-doped CeO$_2$ solids have shown excellent OSC and catalytic performance in many valuable processes.[7−12] MnO$_x$−CeO$_2$ mixed oxides are likely catalysts for oxidation of diesel soot,[7] ethanol, formaldehyde, and phenol[11,12] as well as the selective reaction of NO with NH$_3$.[9] The synergistic interaction between MnO$_x$ and CeO$_2$ seems to play a primary

role in achieving good catalytic activity,[10] making the Mn−Ce oxides very promising candidates as potential industrial catalysts.[8]

It was suggested that Mn^{2+} could be incorporated into the CeO$_2$ lattice due to its size compatibility with that of Ce^{4+}. This incorporation generates structural distortions and electronic changes being the reason for the reduction in the O-vacancy formation energy and contributing to a high catalytic activity.[13] The formation of O-vacancies by the substitution of Mn^{2+} for Ce^{4+} was also proposed in the literature.[13] Mn^{x+} ions, due to their small radius, can enter into the CeO$_2$ lattice and form solid solutions, increasing the amount of oxygen vacancies and thus enhancing the catalytic activity.[7,9] After H$_2$ temperature-programmed reduction (TPR) experiment and reoxidation of MnO$_x$-CeO$_2$ samples, larger reoxidation degrees were attributed to an unsaturated state, with O-vacancies, of the fresh samples.[11] Raman spectroscopy indicates that there are more O-vacancies on the Ce$_{0.88}$Mn$_{0.12}$O$_y$ system than in pure CeO$_2$, which can lead to a higher oxygen mobility from the bulk to the surface.[14]

XPS analysis of Mn-doped CeO$_2$ solid solution as-prepared samples indicates that Mn is mainly present at (3+) oxidation state.[10,15−17] Also, H$_2$-TPR profiles of Ce−Mn$_{(x)}$ were attributed to the reduction from Mn^{3+} to Mn^{2+}.[9,17] Because

Mn^{3+} can only be reduced to Mn^{2+} by O-release, the existence of Mn^{3+}/Mn^{2+} redox couples in $Mn_{0.1}Ce_{0.9}O_x$ is what favors oxygen storage and release during $CO-O_2$ cycles.[17]

In the case of Mn−Ce mixed oxides (molar ratio of Mn:Ce 1:9), one of the O-desorption peaks detected during O_2 temperature-programmed desorption (TPD) tests was attributed to the liberation of lattice oxygen. Further O desorption implies O diffusion from the bulk to the surface and reduction of Mn^{3+} to Mn^{2+} and Ce^{4+} to Ce^{3+}, confirming that Mn incorporation enhances the lattice oxygen mobility.[7] H_2 TPR measurements suggested that $MnO_x−CeO_2$ decreased reduction temperatures compared with those of pure CeO_2 could be attributed to the strong interaction between MnO_x and CeO_2 and the greatly increased oxygen mobility.[18] The mutual promotion effect of CeO_2 and Mn^{3+}/Mn^{2+} species is believed to be essential for the higher dynamic oxygen storage capacity (DOSC) and rate (DOSR) of $Mn_{0.1}Ce_{0.9}O_x$ samples.[17]

Despite the extensive experimental research dedicated to exploring the performance of $MnO_x−CeO_2$ mixed oxides, only a few works have studied, from a fundamental point of view, the influence of Mn−Ce interactions in making these oxides effective catalysts. Tang et al.[19] investigated the redox thermodynamics of doped CeO_2 bulk structure with 3.125 and 6.25% Mn, Pr, Sn, or Zr, obtaining the lowest O-vacancy formation energy for the Mn-doped system. Gupta et al.[15] studied the distortions introduced in the bulk structure of CeO_2 when combined with different metals M (M: Mn, Fe, Co, Ni, Cu), concluding that the longer the M−O bond lengths, the higher the M−Ce mixed oxide OSC. Nonetheless, in their theoretical calculations, the on-site Coulomb interactions for the Ce(4f) and Mn(3d) orbitals as well as spin polarization were not taken into account. Cen et al.[16] evaluated the reduction and reoxidation processes of a CeO_2 (1 1 1) slab in which one of the surface Ce atoms was replaced by Mn. A similar model was employed by Zhang et al.,[14] who reported not only theoretical but also experimental results showing that Mn-doped CeO_2 solid has a higher OSC than pure CeO_2.

Therefore, the aim of this work is to introduce a model that helps to understand the characteristics that make a 12.5% Mn-doped CeO_2 solid solution an efficient oxidation catalyst. We performed density functional theory (DFT+U) calculations to characterize the $Ce_{0.875}Mn_{0.125}O_{1.9375}$(1 1 1) surface, evaluating the influence of the Mn-dopant in the O-vacancy formation, anionic mobility, and redox properties.

2. THEORETICAL METHOD

2.1. Calculation Details. Plane-wave periodic density functional theory (DFT) calculations for the bulk and (1 1 1) surface of Mn-doped CeO_2 were carried out using the Vienna Ab initio Simulation Package VASP.[20,21]

The Kohn−Sham equations were solved with the generalized gradient approximation (GGA) using the exchange-correlation functional of Perdew−Burke−Ernzerhof (PBE).[22] The core electrons were represented with the projector-augmented wave (PAW) method.[23] The valence electron wave functions were expanded using a truncation energy value of 408 eV and a Gaussian smearing of 0.2 eV. We have used the valence configurations $5s^2$, $5p^6$, $6s^2$, $5d^1$, and $4f^1$ for Ce; $3d^6$ and $4s^1$ for Mn; and $2s^2$ and $2p^4$ for O atoms. The Brillouin zone was sampled with $4 \times 4 \times 4$ and $3 \times 2 \times 1$ k-point grids for the bulk and surface structures, respectively, according to the Monkhorst−Pack scheme.[24] For the energy calculations we considered spin-polarization effects. The tolerance for the total

free-energy change was set in 10^{-3} eV, and the final results were extrapolated to those of SIGMA = 0 eV, where SIGMA is the smearing width. Structural relaxations according to the Hellmann−Feynman forces were performed for all of the systems described in this paper. Atomic positions were relaxed until the force acting on each atom was <0.02 eV/Å.

We checked the possible effect on the energetics of surface dipoles by adding a compensating electric field as implemented in the VASP code. Considering this correction, the results were affected in less than 0.02 and 0.05 eV for the formation of a single and double oxygen vacancies on $Ce_{0.875}Mn_{0.125}O_{1.9375}$(1 1 1) surface, respectively. We also checked if taking into account dipole correction would affect the predicted oxidation states of cations, and the results were the same as those obtained for the calculations that included the compensating electric field. According to this, dipole correction was not further considered.

The standard DFT formulation usually fails to describe strongly correlated electrons due to a deficient treatment of electron correlation. This limitation can be corrected by using the DFT+U method, where the introduction of a Hubbard parameter U modifies the self-interaction error and enhances the description of the correlation effects.[25,26] This methodology has been widely used for reduced CeO_2 systems, where the inclusion of the U parameter enhances the description of the strongly correlated Ce(4f) electrons. Nolan et al.,[27] presented periodic density functional theory (DFT+U) calculations of bulk ceria and its low index surfaces (1 1 1), (1 1 0), and (1 0 0). For the study of oxygen vacancy defect formation on the (1 0 0) surface, the cited authors tested values for U in the range of 2−7 eV and found that the degree of delocalization decreases with increasing U. For U < 5 eV, significant delocalization still persisted, while for U = 5 eV and greater, the results were essentially converged. They chose a value of U = 5 eV, which leads to localization of two electrons in the Ce(4f) states for each oxygen vacancy and to an electronic structure corresponding to that observed in experimental UPS spectra.[27] The oxygen vacancy defects in bulk ceria and the low index (1 1 1), (1 1 0), and (1 0 0) surfaces were computed with DFT+U, and the U value was set to 5 eV for all calculations.[28] The calculated offset from the valence band (VB) to the gap state for this U value (5 eV) was 1.1 eV for the (111) surface, and the agreement with the available experimental offset data of 1.2 eV for the reduced (1 1 1) surface was highlighted.[28] The value of U = 5 was also chosen to correctly describe the atomic and electronic structure of both CeO_2 and $CeO_{2−x}$ systems in many other theoretical works.[6,29−31] Zhang et al.[32] performed GGA +U calculations with different U values (2.0, 3.0, 4.0, 5.0, 5.5, 6.0, and 7.0 eV) and found that on the reduced surface with an O vacancy the two excess electrons left behind by the removed O start to become localized at U = 3.0 eV. The degree of localization reaches a maximum at U = 5.0 eV, while for higher U values the charge localization at Ce ions decreases.[32]

Tang et al.[19] in a first-principles investigation on redox properties of Mn-doped CeO_2 used a U value of 4.5 eV for the description of the strong on-site Coulomb repulsion among Mn(3d) electrons. This value removed the self-interaction error and improved the description of the correlation effects. They found that U = 4.5 eV is reasonable by fitting to the experimentally available parameters of MnO, such as lattice constants and band gap.[19] Bayer et al.[33] reported a combined experimental characterization and theoretical study of the formation of Mn_3O_4(0 0 1) on MnO(0 0 1) and studied surface and interface structural stability. From the first-principles

analysis, adopting the value $U = 5.0$ eV for the most favorable Mn_3O_4 surfaces, they obtained energetic arguments for the higher stability of the (0 0 1) orientation.[33] Cen et al.[16] studied the effect of different U values from 0 to 6 eV for Mn(3d) orbitals in the relaxed geometry model of Mn-doped CeO_2. For $U = 0$ eV, the introduction of Mn into the CeO_2(1 1 1) surface made an obvious geometric distortion, which was relieved at $U = 4.5$ eV, resulting in Mn−O bond lengths of 2.22 Å (similar to the experimental bond length of MnO oxide). They also calculated the total density of states for U values from 0 to 4.5 eV and found that the unfilled up-spin gap state goes down and approaches the Fermi level as U increases from 0 to 4.5 eV.[16] Recently, in a first-principles study of SO_2 poisoning effects on pure and Mn-doped CeO_2, the same authors also set the U value to 4.5 eV for Mn(3d) states.[34]

Therefore, in this work we used a Hubbard parameter $U = 5$ eV for Ce(4f) states and $U = 4.5$ eV for the Mn(3d) states because these values are considered to give reliable results.

2.2. Bulk and Surface Models. *2.2.1. Mn-Doped CeO_2 Bulk.* Cerium oxide has a fluorite structure (CaF_2), with a reported experimental value of the lattice parameter of 5.4113 Å (JCPDS #43-1002). The CeO_2 fluorite-type structure consists of a cubic close-packed array of Ce cations with all tetrahedral holes filled by O anions. In this array, each Ce^{4+} cation is surrounded by eight O^{2-} anions that form the corners of a cube. Also, each O^{2-} anion coordinates with four metal cations in a tetrahedron-like structure.

Experimentally, it has been reported that Mn can form solid solutions with CeO_2.[8−10,13,35,36] The limit of MnO_x solubility in CeO_2 was ∼15% Mn cationic content (i.e., Mn/(Ce + Mn) < 0.15).[11,13] Besides, experimental studies showed a slight decrease in the lattice parameter due to 10% Mn mixing into the cerium oxide (5.406,[7] 5.408,[9] and 5.4108 Å[15]).

Thus, our model of Mn-doped CeO_2 contains 12.5% of Mn cations. We employed a cubic supercell formed by 2 × 2 × 2 CeO_2 unit cells (consisting of 32 cations and 64 oxygen atoms), in which four Ce cations were replaced by Mn atoms.

Tang et al.[19] have performed VASP calculations with the on-site Coulomb interaction to study the effect of Mn doping and O-vacancy formation on CeO_2. To study the effect of doping, they replaced one Ce atom by a Mn atom in the same bulk structure as ours and explored different positions for the second dopant atom (from first to fifth nearest-neighbor). As a result, they found that the structures with Mn-dopant placed as first or second nearest-neighbor (NN) were energetically favorable with similar total energies. Taking into account these findings, we introduced the Mn-dopant cations as two pairs of second nearest-neighbors. Simultaneously, these pairs are second nearest-neighbors between each other.

After full relaxation on the bulk structure, our DFT+U calculations resulted in a lattice-constant-optimized value of 5.463 Å for $Ce_{0.875}Mn_{0.125}O_2$ (5.49 Å for pure CeO_2).

We tested other configurations in which two Mn atoms were second nearest-neighbors and the remaining two were 2NN and 2NN; 2NN and 3NN; 2NN and 4NN; 3NN and 3NN; 3NN and 4NN; and 4NN and 4NN. Also, we evaluated the energy of a system with a more regular or isolated distribution, with all Mn cations 4NN between each other (4NN Mn-distributed). All of these configurations, fall in an energy range of ∼0.3 eV, where the last configuration is one of the most stable. However, when O-vacancies were introduced to further stabilize this even configuration, it did not result in the lowest energy system.

Experimental studies have shown that Mn^{2+} ions can selectively substitute the Ce^{4+} cations in the CeO_2 lattice, forming oxygen vacancies to maintain the charge balance.[9] As we have already described in the Introduction, experimental studies indicated that MnO_x−CeO_2 presents structural O-vacancies.[7,9,11,13,14]

Previous simulations of Mn-doped CeO_2 bulk structures have indicated the need for introducing oxygen vacancies near the dopant atom to maintain charge neutrality.[15,19] Moreover, Tang et al. reported that location of the oxygen vacancy at the first neighbor site of Mn is the most stable, with an O-vacancy formation energy of −0.434 eV, resulting in the reduction of Mn^{4+} to Mn^{2+} instead of the usual reduction of Ce^{4+} to Ce^{3+} in pure CeO_2.[19] Following this idea, we decided to remove two oxygen atoms, first nearest-neighbors to two Mn cations, from the systems with different atomic configurations. The energy need for these two O-vacancy formations ($\Delta E_{Bulk2O-Vac.}$) was calculated as:

$$\Delta E_{Bulk2O-vac.} = E[Ce_{0.875}Mn_{0.125}O_{1.9375}] + E[O_2] - E[Ce_{0.875}Mn_{0.125}O_2]$$

where $E[Ce_{0.875}Mn_{0.125}O_{1.9375}]$, $E[Ce_{0.875}Mn_{0.125}O_2]$, and $E[O_2]$ represent the energies of the relaxed bulk structure with and without two oxygen vacancies and molecular oxygen, respectively. The energy of the O-deficient system, consisting of the two pairs of second nearest-neighbors, resulted 0.12 eV lower than that of the O-deficient 4NN Mn-distributed system. Accordingly, we considered that the former configuration (see Figure 1) could be used to describe the O-defective bulk structure.
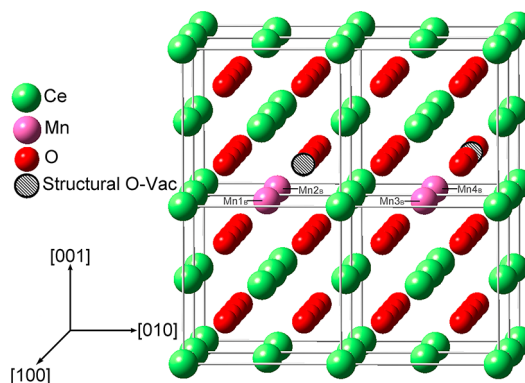
Figure 1. 12.5% Mn-doped 2 × 2 × 2 CeO_2 bulk structure.

The calculations gave a negative value for two O-vacancies formation in the supercell ($\Delta E_{Bulk\ 2O-Vac.} = -2.23$ eV), indicating that Mn-doped CeO_2 solid solution may present oxygen defects in the fluorite-type structure. As a result, the composition of the MnO_x−CeO_2 mixed oxide was $Ce_{0.875}Mn_{0.125}O_{1.9375}$. To determine if the lattice parameter changed with vacancies formation, we performed a reoptimization and found that its value remains the same (5.463 Å).

2.2.2. $Ce_{0.875}Mn_{0.125}O_{1.9375}$(1 1 1) Surface. For cerium oxide, it has been reported that CeO_2(1 1 1) face is one of the most stable.[9,21] This surface corresponds to the minimal Ce−O bonds cleavage. Thus, the $Ce_{0.875}Mn_{0.125}O_{1.9375}$ surface (see Figure 2a,b) was obtained by cleaving the O-defective 2 × 2 × 2 bulk supercell with the (1 1 1) ideal plane, retaining an extra oxygen layer. As shown in Figure 2a, to model the Mn-doped
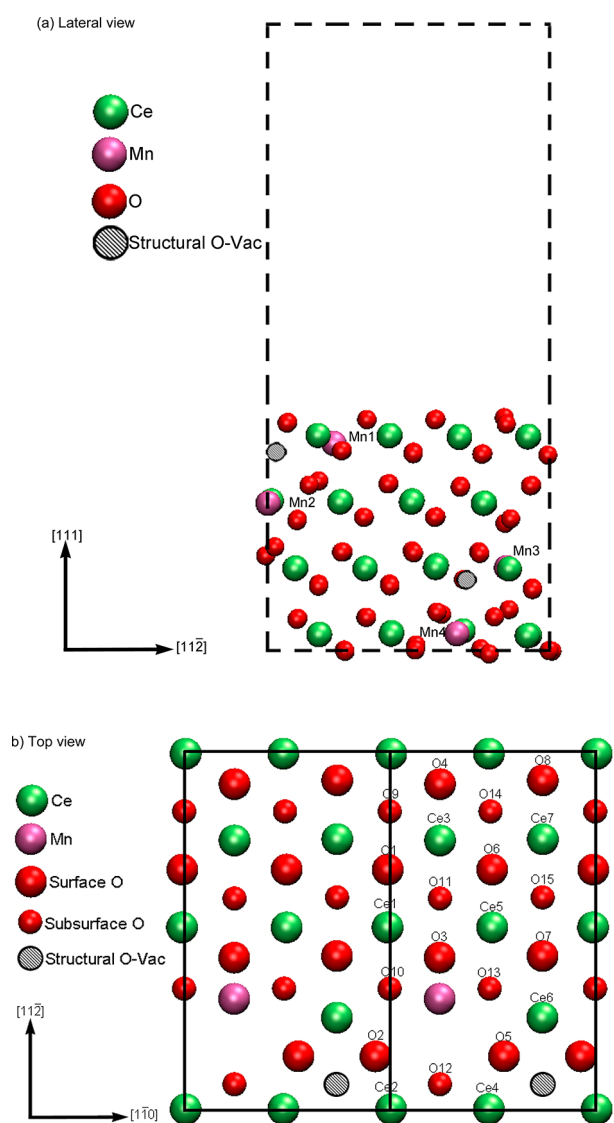
Figure 2. $Ce_{0.875}Mn_{0.125}O_{1.9375}(1\ 1\ 1)$ surface.

CeO_2 (111) surface, we constructed a 12-layer slab. The supercell comprises four Mn-doped CeO_2 trilayers, each of them formed by one O-cations-O sandwich. Modeling the surface as a stack of O-cations-O sandwiches prevents the appearance of a nonzero dipole moment normal to the surface.[37] The two oxygen-terminated surfaces of each side of the Mn-doped ceria slab were separated by a 20 Å thick vacuum space. The latter avoids periodic interactions with the atoms of the upper image.

Calculations on a 24-layer slab showed that it can reproduce the bulk, with surface Mn cations exposing (3+) oxidation state as experimentally reported.[9,10,15−17] Thus, to reduce the system size to a computationally affordable one and take into account the fact that surface O-vacancies affected the oxidation state of inner-layer Mn-dopant cations,[7,9,17,38] we decided for a 12-layer slab with complete relaxation.

Complete optimizations have been previously used to represent active surfaces and their interaction with adsorbates. Nolan et al.[31] studied with a DFT+U approach the geometry and electronic structure of oxygen vacancy defects in the low index (1 1 1), (1 1 0), and (1 0 0) surfaces of ceria. CeO_2 (1 1 1) surface was represented as a 12-layer slab, and the atomic

structure was fully relaxed. Chen et al.[39] studied Au adsorption on (1 1 1) and (1 1 0) surfaces of CeO_2 with a DFT+U approach, modeling the $CeO_2(1\ 1\ 1)$ by a $p(2 \times 2)$ unit cell with 12 layers, in which all of the layers were relaxed. In a combined, experimental and theoretical study of Mn-doped $CeO_2−WO_3$ catalysts, Peng et al.[40] used a four-layer slab, and all layers were fully relaxed. The relaxation of all atoms in the slab was used by Kotomin et al.[41] to model the electronic structure of $LaMnO_3(0\ 0\ 1)$ surface with emphasis on its relaxation for different magnetic configurations. Slabs of different thicknesses, varied from 4 to 12 planes, were used. Piskunov et al.[42] studied electronic structure and thermodynamic stability of $LaMnO_3(0\ 0\ 1)$ and $La_{1-x}Sr_xMnO_3(0\ 0\ 1)$ surfaces, and all atoms have been allowed to relax freely in their simulations. Wörz et al.[43] studied experimentally and via DFT calculations the adsorption of Au atoms on TiO_2 thin films grown on $Mo(1\ 1\ 0)$. They used a four-layer slab of TiO_2 to model this system and optimized the positions of all atoms of the supercell, except those in the bottom. Claeyssens et al.[44] investigated layer-by-layer growth of ZnO by examining computed structures of thin films of ZnO as a function of film thickness. They carried DFT calculations for thickness ranging from 4 to 24 layers and optimized these structures, relaxing all structural degrees of freedom, including the surface lattice vectors.

The full relaxation methodology reported in the literature for similar systems, the presence of surface Mn^{3+}, as experimentally reported, and the economy of computing resources convinced us to use an optimized 12-layer slab as the surface model.

3. RESULTS AND DISCUSSION

3.1. O-Saturated Bulk Structure. After doping, the $2 \times 2 \times 2$ CeO_2 fluorite-type supercell with Mn, whose ionic radius (Mn^{4+}: 0.53 Å, Mn^{3+}: 0.58 Å, Mn^{2+}: 0.83 Å) is smaller than that of Ce^{4+} (0.97 Å),[45] we allowed the system to completely relax to adopt the Ce−O and Mn−O equilibrium bond lengths. In our saturated $Ce_{0.875}Mn_{0.125}O_2$ structure, the calculated Ce−O and Mn−O bonding distances were between 2.36 to 2.38 Å and 2.33 to 2.34 Å, respectively. The symmetry of this structure makes these length intervals very narrow.

The study of the solid electronic structure is essential to understand its redox properties and so to know why the oxidation properties of CeO_2 are enhanced due to Mn-doping. Consequently, density of state (DOS), projected density of states (PDOS), and charge and spin-charge density Bader analysis were employed to study the electronic effects of doping CeO_2 with Mn.

We used Bader charge analysis,[46] to assign ionic oxidation states. But in the case of Mn cation, as it is a high-spin transition metal, its oxidation state can best be determined by integrating the spin-polarization density. This procedure, in comparison with integrating charge density, allows us to filter out the O(2p) contributions.[47] To distinguish between Mn atoms from the bulk and those of the surface, we introduced a subindex B for the atoms of the bulk. So, the notation Mn_B and Mn correspond to Mn atoms in the bulk and in the surface slab, respectively, as shown in Figures 1 and 2a.

The O-saturated $Ce_{0.875}Mn_{0.125}O_2$ bulk structure has a symmetrical disposition of Mn with the same charge over all these cations. Bader charge and spin magnetization of $Mn1_B−Mn4_B$ are shown in Table 1. The charge calculations indicate that Ce cations remained as Ce^{4+}, while all Mn atoms adopted the (3+) oxidation state. The spin-polarized charge density is

Table 1. $Ce_{0.875}Mn_{0.125}O_2$ Bulk Structure Charge Analysis

| cation	Bader charge, e	spin magnetization, μ_B	estimated oxidation state
$Mn1_B$	5.23	4.26	3+
$Mn2_B$	5.23	4.23	3+
$Mn3_B$	5.23	4.23	3+
$Mn4_B$	5.23	4.26	3+

drawn in Figure 3, which shows equally distributed spin density over Mn cations and their coordinated O atoms. Each Mn atom
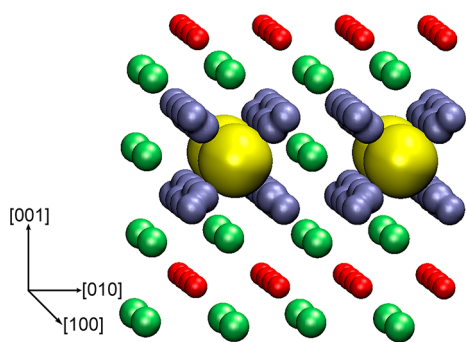
Figure 3. Spin polarization surface at a 0.05 e $Å^{-3}$ isovalue of the relaxed O-saturated 12.5% Mn-doped 2 × 2 × 2 CeO_2 ($Ce_{0.875}Mn_{0.125}O_2$) bulk structure (top view). Positive and negative values are indicated in yellow and gray, respectively.

(majority-spin-polarized) interacts with eight oxygen atoms (minority-spin-polarized), indicating that Mn cations received some electron density from their O-coordination sphere. A similar behavior has been reported for the Mn atom that substituted one surface Ce^{4+} cation in a CeO_2(1 1 1) slab, which was elucidated as O(2p)-holes formation in the oxygen VB.[16]

Meanwhile, the DOS plot of our O-saturated fluorite-type bulk structure shows the conduction band (CB) separated 2.1 eV from the VB, with some peaks in the gap (see Figure 4).
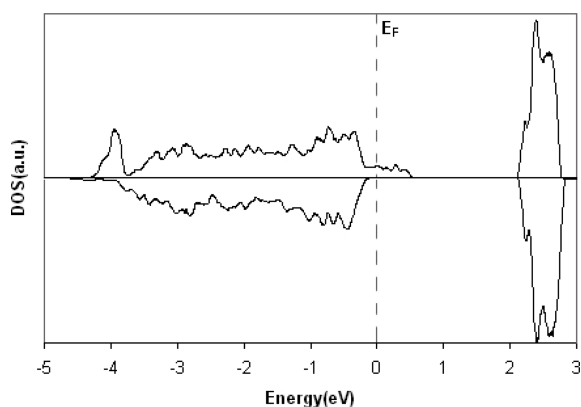
Figure 4. DOS of the O-saturated $Ce_{0.875}Mn_{0.125}O_2$ bulk structure.

These unoccupied states above the Fermi level are mainly formed by O(2p) and Mn(3d) states and could be attributed to the previously mentioned O(2p)-holes creation in the VB.

3.2. O-Defective Structures. *3.2.1. Bulk Structure.* After removing two oxygen atoms in the O-saturated bulk supercell, we allowed the resulting $Ce_{0.875}Mn_{0.125}O_{1.9375}$ structure to fully relax. As we have already mentioned, the formation energy of

two O-vacancies was negative (−2.23 eV), indicating that this system would exhibit structural oxygen defects. In this O-defective bulk, the lengths of Mn−O and Ce−O bonds ranged between 2.03 to 2.51 Å and 2.17 to 2.55 Å, respectively. The distribution of Ce−O distances remained centered in ∼2.37 Å, as in the O-saturated bulk structure (see Figure 5). That is not the case for Mn−O average bond length, which changed from 2.34 to 2.15 Å. Shorter and longer Mn−O bonds appeared as a consequence of the O-vacancies formation. Instead of an eight-fold coordination, characteristic of cations in a fluorite structure, this O-deficient system displays a different arrange of oxygen atoms around Mn cations. After the O-vacancies were introduced, six of the seven remaining oxygen atoms coordinating with $Mn1_B$ and $Mn4_B$ adopted an octahedral arrange around these cations. In both cases, the oxygen atoms excluded from the new atomic configuration are at a 2.86 Å distance from these cations. The situation is different for $Mn2_B$ and $Mn3_B$, which have shorter bond lengths with four oxygen atoms (2.16 to 2.51 Å), while bond lengths with the other four oxygen atoms are longer (2.65 to 2.76 Å).

The O-defective bulk structure with two O-vacancies gave place to the presence of Mn atoms with different oxidation states. As can be seen in Table 2, the assigned oxidation states of $Mn2_B$ and $Mn3_B$ were (2+); while that for $Mn1_B$ and $Mn4_B$ was (4+). Meanwhile, Ce atoms maintained an integrated charge density of 9.6 e, indicating that Ce atoms did not undergo reduction despite the presence of the two bulk O-vacancies. Figure 6 shows the four Mn atoms majority-spin-polarized. Two of these cations ($Mn2_B$ and $Mn3_B$) coordinate with four nonpolarized O atoms each, denoting that the O(2p) orbitals are filled. This description agrees with the assignment of (2+) oxidation state to $Mn2_B$ and $Mn3_B$ cations.

Consequently, the DOS plot (Figure 7) shows these occupied $Mn2_B$(3d)-O(2p) and $Mn3_B$(3d)-O(2p) states on and below the Fermi level. This picture indicates that the electron density left behind by the O-removal could be transferred to those Mn cations, whereas each of the other two Mn cations of Figure 6 ($Mn1_B$ and $Mn4_B$), with a formal charge of (4+), coordinate with six minority spin polarized oxygen atoms. In the DOS curve, localized gap peaks can be seen associated with $Mn1_B$(3d)-O(2p) and $Mn4_B$(3d)-O(2p) unoccupied states.

For completeness, we evaluated Mn oxidation states of the O-deficient 4NN Mn-distributed system (0.12 eV less stable than the chosen configuration) and found that the formation of two O-vacancies on this isolated Mn cation substitution resulted in (3+) for all Mn-dopant cations.

3.2.2. Surface Structure. The $Ce_{0.875}Mn_{0.125}O_{1.9375}$(1 1 1) surface was obtained by the cleavage of the O-defective bulk structure with the (1 1 1) plane. The formation of this surface led to Mn−O and Ce−O bond length intervals between 1.92 to 2.55 Å and 2.14 to 2.55 Å, respectively. The average value and distribution of Ce−O bond lengths were similar to those in the previously analyzed bulk systems. However, the distribution of Mn−O bond lengths became modified due to the formation of the surface, and the average value changed from 2.15 (in the O-defective bulk structure) to 2.08 Å (see Figure 5). The topmost Mn-dopant cation adopted very short bonds with its diminished four-fold oxygen coordination sphere, descending 0.30 Å beneath the surface.

Spin Bader analysis indicates that surface Mn cations would be in (3+) oxidation state (see Table 2). Concomitantly, the DOS curve of the $Ce_{0.875}Mn_{0.125}O_{1.9375}$(1 1 1) surface shows

(a) Ce-O bond lengths
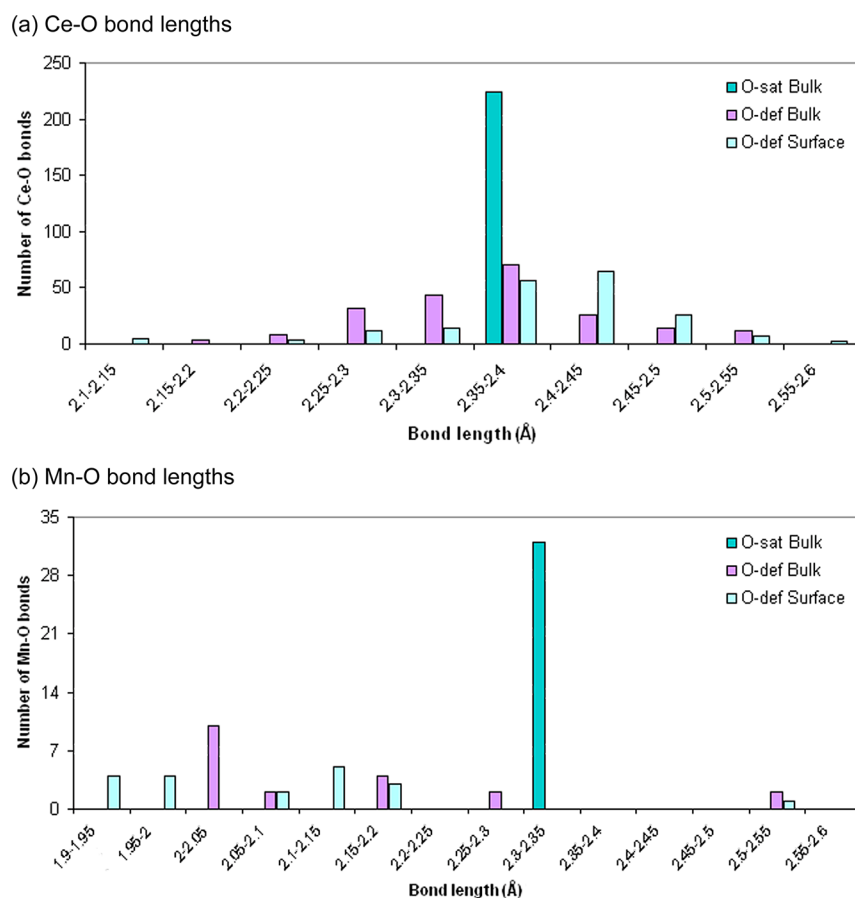

(b) Mn-O bond lengths

Figure 5. Cation-O bond lengths in the O-saturated $Ce_{0.875}Mn_{0.125}O_2$ bulk structure and O-defective $Ce_{0.875}Mn_{0.125}O_{1.9375}$ bulk and surface structures.

Table 2. O-Defective $Ce_{0.875}Mn_{0.125}O_{1.9375}$ Systems Charge Analysis

system	cation	Bader charge, e	spin magnetization, μ_B	estimated oxidation state
O-defective bulk structure	$Mn1_B$	4.98	3.57	4+
	$Mn2_B$	5.39	4.84	2+
	$Mn3_B$	5.39	4.84	2+
	$Mn4_B$	4.98	3.57	4+
O-defective (1 1 1) surface	Mn1	5.15	4.00	3+
	Mn2	5.15	4.16	3+
	Mn3	5.15	4.15	3+
	Mn4	5.15	4.13	3+
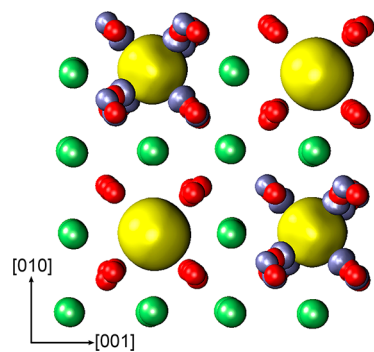
Figure 6. Spin polarization surface at a 0.05 e $Å^{-3}$ isovalue of the relaxed O-deficient 12.5% Mn-doped 2 × 2 × 2 CeO_2 ($Ce_{0.875}Mn_{0.125}O_{1.9375}$) bulk structure (top view). Positive and negative values are indicated in yellow and gray, respectively.
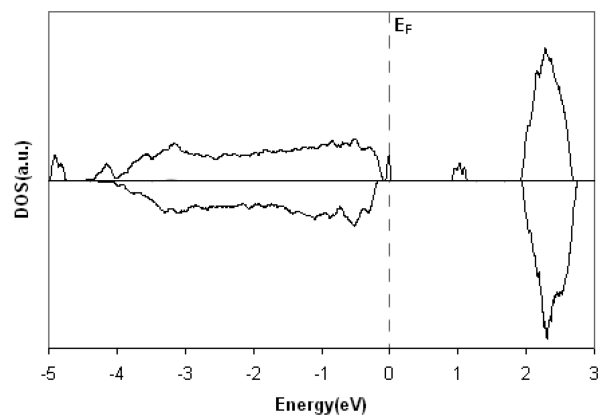
Figure 7. DOS plot of the O-defective $Ce_{0.875}Mn_{0.125}O_{1.9375}$ bulk.

18068

dx.doi.org/10.1021/jp403911b | J. Phys. Chem. C 2013, 117, 18063−18073

several localized unoccupied gap states associated with the contribution of Mn(3d)−O(2p) states (see Figure 8). The

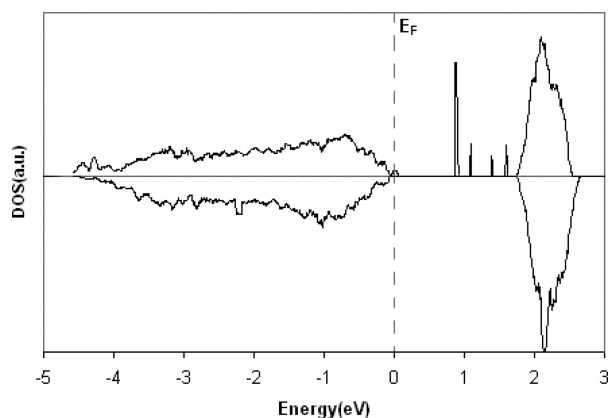**Figure 8.** DOS plot of the $Ce_{0.875}Mn_{0.125}O_{1.9375}(1\ 1\ 1)$ slab.

presence of unfilled gap states coming from Mn^{3+} cations was also observed in the DOS plot of O-saturated bulk structure. However, it should be noted that the latter curve shows the unoccupied Mn(3d)−O(2p) peaks distributed in a continuous narrow range of energy above the Fermi level (see Figure 4).

3.3. Formation of O-Vacancies on the $Ce_{0.875}Mn_{0.125}O_{1.9375}$ (1 1 1) Surface. *3.3.1. Single O-Vacancy.* To study the ease of $Ce_{0.875}Mn_{0.125}O_{1.9375}(1\ 1\ 1)$ surface reduction and its electronic implications, we performed energy structure calculations for an O-vacancy formation on different surface sites.

In Figure 2b, we can see that the catalyst surface exhibits O atoms with different neighboring cations. The oxygen O3 coordinates with Mn and Ce cations, while O2, O5, and O8, despite not coordinating with a Mn-dopant, are in its vicinity and near a structural O-vacancy. Finally, O1, O4, and O6 coordinate with Ce cations and are distant to Mn-dopant or structural O-defects. Thus, we study the formation of an O-vacancy by removing O2, O3, and O4 atoms because they represent the different possible surface oxygen sites.

The energy required to form a surface O-vacancy ($\Delta E_{Surf.O-Vac.}$) was calculated as:

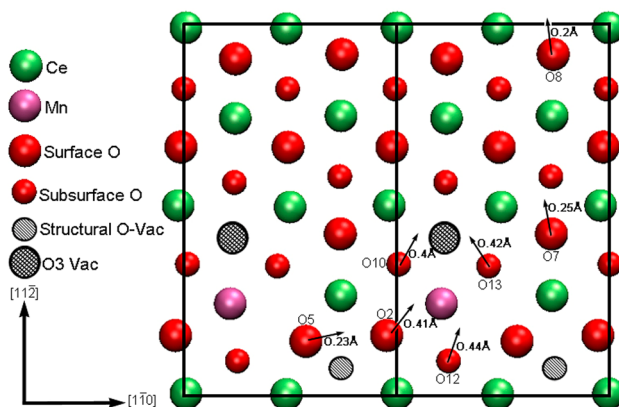$$\Delta E_{Surf.O-Vac.} = E[OVac\text{-}Ce_{0.875}Mn_{0.125}O_{1.9375}(111)]$$
$$\frac{1}{2}E[O_2] - E[Ce_{0.875}Mn_{0.125}O_{1.9375}(111)]$$

where $E[Ce_{0.875}Mn_{0.125}O_{1.9375}(1\ 1\ 1)]$, $E[OVac\text{-}Ce_{0.875}Mn_{0.125}O_{1.9375}(1\ 1\ 1)]$, and $E[O_2]$ are the energies of the relaxed (1 1 1) surface slabs before and after introducing a surface O-vacancy and the energy of the O molecule in vacuum, respectively. Note that in this case positive values indicate that energy is needed to form the O-vacancies.

The calculated energy values for O4-, O3-, and O2-defect creation were 0.38, 0.66, and 0.77 eV, respectively. A correlation was noticed between the O-vacancy formation energy (O4 < O3 < O2) and the average O-metal cation bond lengths, which are 2.33, 2.23, and 2.15 Å, respectively.

To understand the influence of Mn in the mobility of the oxygen atoms of the system, we studied the anionic displacements after performing these surface O vacancies. Figures 9 and 10 show the final position of the anions after removing O3 and O4, respectively. The arrows indicate the
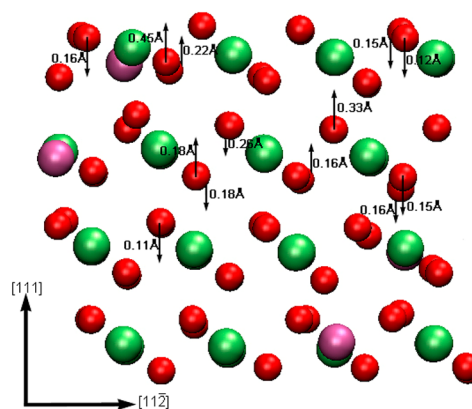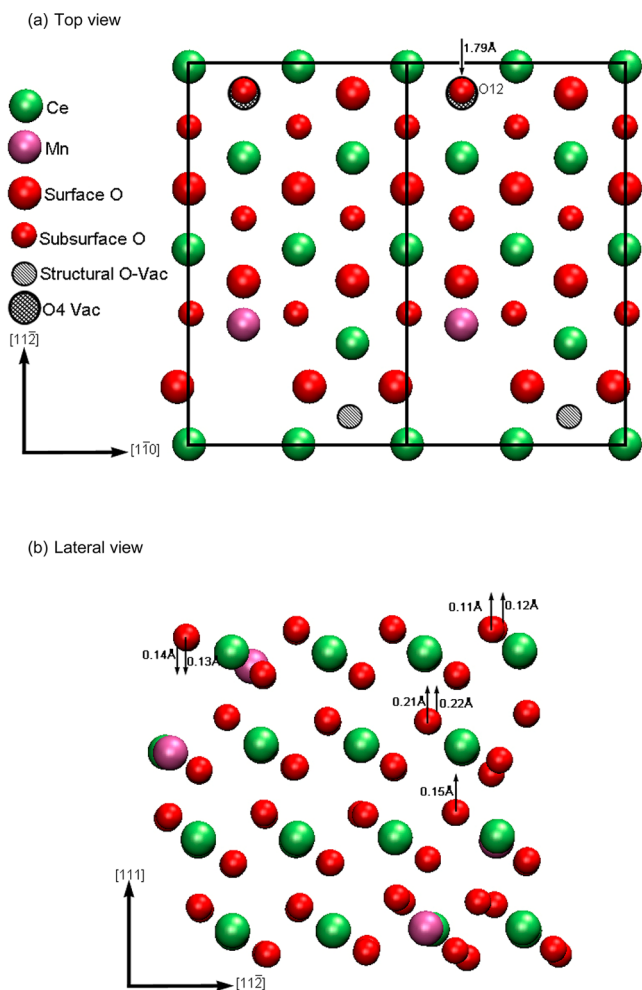

Figure 9. $Ce_{0.875}Mn_{0.125}O_{1.9375}(1\ 1\ 1)$ slab without O3. The arrows indicate the direction of displacement for the atoms from their original position in $Ce_{0.875}Mn_{0.125}O_{1.9375}(1\ 1\ 1)$.

direction of the displacement of these oxygen atoms from their original position in the $Ce_{0.875}Mn_{0.125}O_{1.9375}(1\ 1\ 1)$ system. When O3-vacancy was performed, many neighboring surface and subsurface O-atoms (see Figure 9a) suffered strong relaxations while displacing toward the hole left by the O-removal. As can be seen in Figure 9b, inner O-atoms also moved considerably. Meanwhile, after O4 removal, its hole is directly replenished by O12 (see Figure 10a), which suffers a very significant displacement of 1.79 Å toward O4 original position. Figure 10b, shows less inner oxygen movements due to O4 removal than in the case of O3-vacancy formation. Note that in both single surface oxygen vacancy formations, O3- or O4-defect, neighboring surface and inner O atoms moved toward the hole corresponding to that O-defect.

We performed charge analysis on the O-defective slab with a single surface O-vacancy to obtain some electronic information of the reduced $Ce_{0.875}Mn_{0.125}O_{1.9375}(1\ 1\ 1)$ surface. On one hand, when O3 was removed, Mn1 and Mn2 went reduced from Mn^{3+} to Mn^{2+} (see Table 3). The density of states indicates that the peaks corresponding to the unoccupied Mn1(3d) and Mn2(3d) states, located in the gap, disappear after making the O3-vacancy (see Figure S1a,b, Supporting Information).

On the other hand, when O4 was removed, Mn2 and Mn3 became reduced (see Table 3) and adopted the (2+) oxidation state. The corresponding projected DOS plot of Mn2(3d) and Mn3(3d) orbitals also showed the disappearance of these

(a) Top view

(b) Lateral view

Figure 10. $Ce_{0.875}Mn_{0.125}O_{1.90625}(1\ 1\ 1)$ system without O4. The arrows indicating the direction of displacements for the atoms from their original position in $Ce_{0.875}Mn_{0.125}O_{1.9375}(1\ 1\ 1)$.

empty states due to the O3 removal (Figure S2a,b, Supporting Information). We also noticed that the reduction of Mn1, Mn2, and Mn3 cations to Mn^{2+} has a consequential formation of new Mn(3d) states at the Fermi level.

This calculation was also performed on the same slab with three and six fixed layers. For the slab with six fixed layers, a surface Ce cation, instead of Mn3, underwent reduction. However, for the slab with three fixed layers, no changes in location of Mn^{2+} and Mn^{3+} were observed, evidencing the reduction of Mn before that of Ce cations, which agrees with experimental reported H_2-TPR results.[8]

3.3.2. Double O-Vacancies. According to the energy values calculated for a surface O-defect creation on the $Ce_{0.875}Mn_{0.125}O_{1.9375}(1\ 1\ 1)$ slab, O4 and O3 would be the first and second most favorable oxygen atoms to be released by this system. To study the easy of performing a second O-defect, we removed O3 from the surface with O4 vacancy. Thus, the O3-vacancy formation energy after O4 was already removed ($\Delta E_{Surf.2O\text{-}Vac.}$) was calculated as:

$$\Delta E_{Surf.2O\text{-}Vac.} = E[2OVac\text{-}Ce_{0.875}Mn_{0.125}O_{1.9375}(111)]$$
$$+ \frac{1}{2}E[O_2]$$
$$- [OVac\text{-}Ce_{0.875}Mn_{0.125}O_{1.9375}(111)]$$

where $E[2OVac\text{-}Ce_{0.875}Mn_{0.125}O_{1.9375}(1\ 1\ 1)]$, $E[OVac\text{-}Ce_{0.875}Mn_{0.125}O_{1.9375}(1\ 1\ 1)]$, and $E[O_2]$ are the energies of the relaxed surface slabs with O4- and O3-vacancies, O4-vacancy, and the energy of the O_2 molecule in vacuum, respectively.

With this calculation, we obtained a value of 2.28 eV for the second surface O-defect creation. Similarly to the formation of a single-surface O3-vacancy, the removal of O3 after that of O4 led to a similar O-mobility pattern. We found analogous oxygen displacements in the surface, subsurface, and inner layers in both cases.
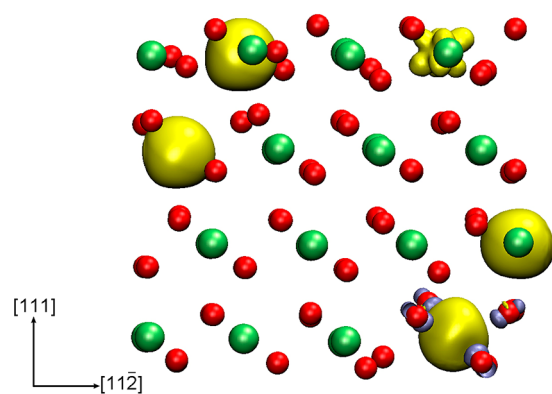
Concerning the electronic implications of two surface O-vacancies formation (O4 and O3), we notice that not only three Mn cations but also one surface Ce became reduced. The Bader analysis of spin density shown in Table 4 indicates that

Table 4. Charge Analysis of the O-Defective $Ce_{0.875}Mn_{0.125}O_{1.9375}(1\ 1\ 1)$ Slab with Two Surface O-Vacancies

| cation	Bader charge, e	spin magnetization, μ_B	estimated oxidation state
Mn1	5.46	4.80	2+
Mn2	5.41	4.82	2+
Mn3	5.40	4.84	2+
Mn4	5.13	4.00	3+
Ce3	9.94	0.98	3+

Mn1, Mn2, and Mn3 were in the (2+) oxidation state, while Ce3 (see the label in Figure 2b) was reduced to Ce^{3+}. The net spin isosurface shown in Figure 11 evidences the characteristic spin-majority spatial distribution of Ce3(4f) orbitals, which is similar to that found for Ce^{3+} in CeO_2.[16,27,31] Figure 11 also evidence the difference in charge between Mn cations of the first three cationic layers (Mn1, Mn2, and Mn3: Mn^{2+}) and Mn4 (Mn^{3+}).

Table 3. Charge Analysis of the O-Defective $Ce_{0.875}Mn_{0.125}O_{1.9375}(1\ 1\ 1)$ Slab with a Single Surface O-Vacancy

system	cation	Bader charge, e	spin magnetization, μ_B	estimated oxidation state
O3-vacancy	Mn1	5.41	4.81	2+
	Mn2	5.42	4.81	2+
	Mn3	5.13	4.19	3+
	Mn4	5.14	4.03	3+
O4-vacancy	Mn1	5.16	3.99	3+
	Mn2	5.46	4.81	2+
	Mn3	5.40	4.83	2+
	Mn4	5.15	4.13	3+

Figure 11. Spin polarization surface at a 0.05 e Å^{-3} isovalue of the $Ce_{0.875}Mn_{0.125}O_{1.9375}$(1 1 1) surface without O3 and O4 (lateral view). Positive and negative values are indicated in yellow and gray, respectively.

The DOS curve for the $Ce_{0.875}Mn_{0.125}O_{1.9375}$(1 1 1) surface with O4- and O3-vacancies (see Figure 12) shows the Ce3(4f)
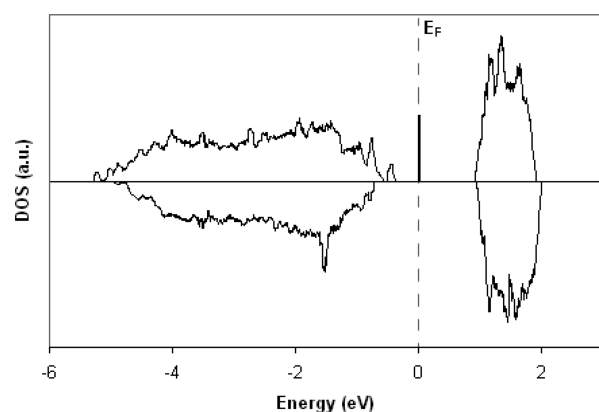
Figure 12. DOS plot of the O-defective $Ce_{0.875}Mn_{0.125}O_{1.9375}$(1 1 1) surface without O3 and O4.

states on the Fermi level and the localized Mn(3d) peak, corresponding to Mn4 cation in (3+) oxidation state, very close to the bottom of the CB. Note that there are not localized Mn1, Mn2, and Mn3 unoccupied Mn(3d) gap states, which disappeared after making the O4- and O3-vacancies.

3.4. Discussion. The doping of CeO_2 fluorite-type structure with 12.5% (cationic content) of Mn resulted in a slight reduction of its lattice parameter from 5.49 to 5.463 Å, which accords with reported experimental data noticing a small lattice parameter shrinkage for MnO_x−CeO_2 solid solutions.[7,9]

The O-saturated bulk structure showed modifications in Ce−O bond lengths, which changed from the regular pattern of 2.34 Å to longer bonds in the 2.36 to 2.38 Å range. According to our spin-polarized electronic analysis, Ce atoms were present as Ce^{4+}, while Mn cations adopted the (3+) oxidation state. The origin of these Mn^{3+} cations could lie in some O(2p)−Mn(3d) charge transference, with the consequential formation of O(2p) holes in the VB.[16] This charge donation was reflected as unfilled gap states just above the Fermi level of our DOS plot.

The formation of two O-vacancies in the 12.5% Mn-doped CeO_2 solid solution resulted in a more stable bulk structure ($\Delta E_{Bulk\ 2O-Vac}$= −2.23 eV), with two Mn-dopant ions adopting Mn^{2+} and Mn^{4+} states in each case. In addition, Ce cation oxidation state remained unchanged despite the creation of two

bulk O-vacancies. Concerning the DOS plot of the O-defective bulk structure, we observed changes in the electronic structure of the host CeO_2 lattice mainly due to the presence of new states coming from Mn(3d)−O(2p) interactions. There are unfilled states located at the gap corresponding to Mn^{4+} cations and occupied states at the Fermi level formed by contributions of the reduced Mn^{2+} ions.

The stability of our O-defective bulk structure is in accordance with reported experimental studies, which have shown that Mn^{2+} ions selectively substitute the Ce^{4+} sites, causing the formation of oxygen vacancies in Ce−Mn mixed oxides with a low Mn content.[9] The authors argued that Mn^{2+} cations with similar ionic radius to that of Ce^{4+} (0.83 and 0.97 Å, respectively[45]) can occupy the Ce^{4+} sites by isomorphous substitution forming oxygen vacancies to maintain the charge balance. The presence of lattice O-defects is also supported by other experimental works.[7,11,13,14]

The creation of the (1 1 1) surface was accompanied by an important atomic relaxation with the consequential charge redistribution, changing the oxidation state of surface Mn atoms to (3+). The topmost Mn-dopant cation adopted short bonds with its diminished four-fold oxygen coordination sphere modifying its oxidation state to Mn^{3+}, whose ionic radius is smaller than that of Ce^{4+} (0.58 and 0.97 Å, respectively). Therefore, the other Mn cations, which have five-fold coordination, also changed to Mn^{3+} to maintain the electroneutrality of the slab. The presence of Mn^{3+} species in our surface model accords with the indications of experimental measurements for Mn−Ce mixed oxides with various Mn contents, showing that Mn^{3+} cations seem to occupy the surface sites of CeO_2 crystals,[10,11,15−17,48] whereas the DOS curve of the $Ce_{0.875}Mn_{0.125}O_{1.9375}$(1 1 1) slab shows unfilled Mn(3d)-O(2p) gap states. The presence of these states could involve some O(2p)−Mn(3d) charge transfer, suggesting the formation of surface-activated oxygen species. In this regard, it has been reported that strong Mn−Ce interactions and high average oxidation number of Mn and Ce ions greatly promote reactive surface oxygen availability in $MnCeO_x$ catalyst.[38]

The formation of a single O-vacancy on the $Ce_{0.875}Mn_{0.125}O_{1.9375}$(1 1 1) surface was easy ($\Delta E_{Surf.O-Vac.}$ = 0.38 eV) and lead to strong geometric relaxation of subsurface and inner-layer oxygen atoms. When an O atom (O3) coordinating with a Mn cation (Mn1) was removed, we detected high surface and inner anionic movements toward the hole left by this removal. When an O atom (O4) not so close to Mn1 was removed, we observed less average anionic movement, but an oxygen near-neighbor to Mn1 adopted the original O4 position. These facts suggest that Mn-doped CeO_2 would release more easily those O atoms neighboring Mn cations, increasing the oxygen surface availability and anionic mobility.

In addition, the formation of a single surface O-defect was accompanied by the reduction of two Mn^{3+} cations to Mn^{2+}. Previous theoretical works[6,49] have shown that creation of surface O-vacancies in Zr-doped CeO_2(1 1 1) slab resulted in reduction of Ce^{4+} cations to Ce^{3+}. However, Mn has a high reduction/oxidation facility and presents several oxidation states,[7] and thus the excess two electrons left by a single O-vacancy creation in the $Ce_{0.875}Mn_{0.125}O_{1.9375}$(1 1 1) surface could occupy the Mn(3d) states instead of the Ce(4f) states. Therefore, the half occupation of Mn(3d) states resulted in the formation of stable Mn^{2+} ions.[19,50]

18071

dx.doi.org/10.1021/jp403911b | *J. Phys. Chem. C* 2013, 117, 18063−18073

Moreover, we found that the energy required for the formation of two surface oxygen defects on the $Ce_{0.875}Mn_{0.125}O_{1.9375}(1\ 1\ 1)$ slab was similar to that needed for the creation of a single surface O-vacancy on $CeO_2(1\ 1\ 1)$ (2.66 vs 2.69 eV, respectively).

After this second O-vacancy formation, three Mn cations became reduced to Mn^{2+}, and also one Ce atom underwent reduction to Ce^{3+}. Noticeably, one of the Mn cations and the Ce atom are surface nearest-neighbors of the removed oxygen atoms, while the other two Mn cations are located on the second and third cationic layers. This result is in accordance with experimental reports about the surface O-vacancy effect on the oxidation state of inner-layer Mn-dopant cations[7,9,17,38] and could be observed due to our model including structural O-defects and Mn atoms in all cationic layers. It evidenced high oxygen mobility and reduction of three Mn cations and one Ce atom after the formation of double-surface O-defect.

Our calculations showed that Mn-dopant reduced the energy required for creation of O-vacancies in $CeO_2(1\ 1\ 1)$ surface, which led to the formation of Mn^{3+}/Mn^{2+} pairs and reduction of a Ce^{4+} cation to Ce^{3+} only after further surface O-defects formation. This result suggests a synergistic effect between MnO_x and CeO_2 centers and accords with combined H_2-TPR and XPS data showing that reduction of Mn^{3+} and Ce^{4+} cations in $Ce_{0.9}Mn_{0.1}O_{2-\delta}$ was shifted to lower temperature compared with that in Mn_2O_3 and CeO_2, respectively.[15]

4. CONCLUSIONS

In this work, we performed DFT+U periodic calculations to characterize in detail the 12.5% Mn-doped CeO_2 solid solution. The calculations indicated that Mn^{2+} cations could substitute Ce^{4+} ions, leading to the formation of structural O-vacancies in the host CeO_2 lattice. Charge redistribution occurred upon the creation of the $Ce_{0.875}Mn_{0.125}O_{1.9375}(1\ 1\ 1)$ surface, where Mn adopted the Mn^{3+} charge state.

The formation of a single O-vacancy on $Ce_{0.875}Mn_{0.125}O_{1.9375}(1\ 1\ 1)$ surface was much easier than that on $CeO_2(1\ 1\ 1)$, which could be related to Ce−O bond enlargement because of Mn doping, and two Mn cations became reduced. Even more, the creation of two oxygen vacancies on the Mn-doped $CeO_2(1\ 1\ 1)$ surface required similar energy to that for the formation of a single O-vacancy on the bare host surface. Noticeably, the double O-removal led to the reduction of three Mn cations and also one Ce atom. In both single and double O-vacancy formation cases, surface and inner-layer oxygen atoms experienced important relaxations as moving to the hole left by those vacancies.

Our results evidence the effect of Mn-dopant in promoting the formation of structural O-defects, surface active oxygen atoms release, and bulk anionic mobility and could help to explain the significant performance of Mn-doped CeO_2 in oxidation reactions.

ASSOCIATED CONTENT

ⓢ Supporting Information

Projected DOS plot of Mn(3d) orbitals in the O3-defective $Ce_{0.875}Mn_{0.125}O_{1.9375}(1\ 1\ 1)$ surface showing Mn1(3d) and Mn2(3d) orbitals. Projected DOS plot of Mn(3d) orbitals in the O4-defective $Ce_{0.875}Mn_{0.125}O_{1.9375}(1\ 1\ 1)$ surface showing Mn2(3d) and Mn3(3d) orbitals. This material is available free of charge via the Internet at http://pubs.acs.org.

AUTHOR INFORMATION

Corresponding Author
*E-mail: beatriz@di.fcen.uba.ar.

Notes
The authors declare no competing financial interest.

REFERENCES

(1) Trovarelli, A. *Catalysis by Ceria and Related Materials*; Imperial College Press: London, U.K., 2002.

(2) Aneggi, E.; Boaro, M.; Leitenburg, C.; Dolcetti, G.; Trovarelli, A. Insights into the Redox Properties of Ceria-based Oxides and Their Implications in Catalysis. *J. Alloys Compd.* **2006**, *408*, 1096−1102.

(3) Kašpar, J.; Fornasiero, P.; Graziani, M. Use of CeO_2-based Oxides in the Three-way Catalysis. *Catal. Today* **1999**, *50*, 285−298.

(4) Zhang, C. J.; Michaelides, A.; King, D. A.; Jenkins, S. J. Oxygen Vacancy Clusters on Ceria: Decisive Role of Cerium f Electrons. *Phys. Rev. B* **2009**, *79*, 075433(1−11).

(5) Dholabhai, P. P.; Adams, J. B.; Crozier, P.; Sharma, R. Oxygen Vacancy Migration in Ceria and Pr-doped Ceria: A DFT+U study. *J. Chem. Phys.* **2010**, *132*, 094104(1−8).

(6) Yang, Z.; Wei, Y.; Fu, Z.; Hermansson, K. Facilitated Vacancy Formation at Zr-Doped Ceria(1 1 1) surfaces. *Surf. Sci.* **2008**, *602*, 1199−1206.

(7) Liang, Q.; Wu, X.; Weng, D.; Xu, H. Oxygen Activation on Cu/Mn-Ce Mixed Oxides and the Role in Diesel Soot Oxidation. *Catal. Today* **2008**, *139*, 113−118.

(8) Chen, H.; Sayari, A.; Adnot, A.; Larachi, F. Composition-Activity Effects of Mn-Ce-O Composites on Phenol Catalytic Wet Oxidation. *Appl. Catal., B* **2001**, *32*, 195−204.

(9) Hong, W.; Iwamoto, S.; Hosokawa, S.; Wada, K.; Kanai, H.; Inoue, M. Effect of Mn Content on Physical Properties of CeO_x-MnO_y Support and BaO-CeO_x-MnO_y Catalysts for Direct NO Decomposition. *J. Catal.* **2011**, *277*, 208−216.

(10) Delimaris, D.; Ioannides, T. VOC Oxidation Over MnO_x-CeO_2 Catalysts Prepared by a Combustion Method. *Appl. Catal., B* **2008**, *84*, 303−312.

(11) Shan, W.; Ma, N.; Yang, J.; Dong, X.; Liu, C.; Wei, L. Catalytic Oxidation of Soot Particulates over MnO_x-CeO_2 Oxides Prepared by Complexation-Combustion Method. *J. Nat. Gas Chem* **2010**, *19*, 86−90.

(12) Abecassis-Wolfovich, M.; Jothiramalingam, R.; Landau, M. V.; Herskowitz, M.; Viswanathan, B.; Varadarajan, T. K. Cerium Incorporated Ordered Manganese Oxide OMS-2 Materials: Improved Catalysts for Wet Oxidation of Phenol Compounds. *Appl. Catal., B* **2005**, *59*, 91−98.

(13) Kang, C. H. Y.; Kusaba, H.; Yahiro, H.; Sasaki, K.; Teraoka, Y. Preparation, Characterization and Electrical Property of Mn-Doped Ceria-Based Oxides. *Solid State Ionics* **2006**, *177*, 1799−1802.

(14) Zhang, M.; Jiang, D.; Jiang, H. Enhanced Oxygen Storage Capacity of $Ce_{0.88}Mn_{0.12}O_y$ Compared to CeO_2: An Experimental and Theoretical Investigation. *Mater. Res. Bull.* **2012**, *47*, 4006−4012.

(15) Gupta, A.; Waghmare, U. V.; Hegde, M. S. Correlation of Oxygen Storage Capacity and Structural Distortion in Transition-Metal-, Noble-Metal-, and Rare-Earth-Ion-Substituted CeO_2 from First Principles Calculation. *Chem. Mater.* **2010**, *22*, 5184−5198.

(16) Cen, W.; Liu, Y.; Wu, Z.; Wang, H.; Weng, X. A Theoretic Insight into the Catalytic Activity Promotion of CeO_2 Surfaces by Mn Doping. *Phys. Chem. Chem. Phys.* **2012**, *14*, 5769−5777.

(17) Jia, L.; Shen, J.; Wang, J.; Gu, W. Dynamic Oxygen Storage and Release over $Cu_{0.1}Ce_{0.9}Ox$ and $Cu_{0.1}Ce_{0.6}Zr_{0.3}Ox$ Complex Compounds and Structural Characterization. *J. Alloys Compd.* **2009**, *473*, 293–297.

(18) Shi, L.; Chu, W.; Qu, F.; Hu, J.; Li, M. Catalytic Performance for Methane Combustion of Supported Mn-Ce Mixed Oxides. *J. Rare Earths* **2008**, *26*, 836–840.

(19) Tang, Y.; Zhang, H.; Cui, L.; Ouyang, C.; Shi, S.; Tang, W.; Li, H.; Lee, J.; Chen, L. First-Principles Investigation on Redox Properties of M-doped CeO_2 (M=Mn,Pr,Sn,Zr). *Phys. Rev. B* **2010**, *82*, 125104(1–9).

(20) Kresse, G.; Furthmuller, J. Efficiency of Ab-initio Total Energy Calculations for Metals and Semiconductors Using a Plane-Wave Basis Set. *Comput. Mater. Sci.* **1996**, *6*, 15–50.

(21) Kresse, G.; Hafner, J. Ab Initio Molecular Dynamics for Liquid Metals. *Phys. Rev. B* **1993**, *47*, 558–561.

(22) Perdew, J.; Burke, K.; Ernzerhof, M. Generalized Gradient Approximation Made Simple. *Phys. Rev. Lett.* **1996**, *77*, 3865–3868.

(23) Kresse, G.; Joubert, D. From Ultrasoft Pseudopotentials to the Projector Augmented-wave Method. *Phys. Rev. B* **1999**, *59*, 1758–1775.

(24) Monkhorst, H.; Pack, J. Special Points for Brillouin-Zone Integrations. *Phys. Rev. B.* **1976**, *13*, 5188–5192.

(25) Dudarev, S.; Botton, G.; Savrasov, S.; Humphreys, C.; Sutton, A. Electron-Energy-Loss Spectra and the Structural Stability of Nickel Oxide: An LSDA+U Study. *Phys. Rev. B* **1998**, *57*, 1505–1509.

(26) Anisimov, V.; Zaanen, J.; Andersen, O. Band Theory and Mott Insulators: Hubbard U Instead of Stoner I. *Phys. Rev. B* **1991**, *44*, 943–954.

(27) Nolan, M.; Grigoleit, S.; Sayle, D.; Parker, S.; Watson, G. Density Functional Theory Studies of the Structure and Electronic Structure of Pure and Defective Low Index Surfaces of Ceria. *Surf. Sci.* **2005**, *576*, 217–229.

(28) Nolan, M.; Fearon, J. E.; Watson, G. W. Oxygen Vacancy Formation and Migration in Ceria. *Solid State Ionics* **2006**, *177*, 3069–3074.

(29) Li, H.; Wang, H.; Gong, X.; Guo, Y.; Guo, Y.; Lu, G.; Hu, P. Multiple Configurations of the Two Excess 4f Electrons on Defective $CeO_2(1\ 1\ 1)$: Origin and Implications. *Phys. Rev. B* **2009**, *79*, 193401(1–4).

(30) Castleton, C.; Kullgren, J.; Hermansson, K. Tuning LDA+U for Electron Localization and Structure at Oxygen Vacancies in Ceria. *J. Chem. Phys.* **2007**, *127*, 244704(1–11).

(31) Nolan, M.; Parker, S.; Watson, G. The Electronic Structure of Oxygen Vacancy Defects at the Low Index Surfaces of Ceria. *Surf. Sci.* **2005**, *595*, 223–232.

(32) Zhang, C.; Michaelides, A.; King, D. A.; Jenkins, S. J. Anchoring Sites for Initial Au Nucleation on $CeO_2\{1\ 1\ 1\}$: O Vacancy versus Ce Vacancy. *J. Phys. Chem. C* **2009**, *113*, 6411–6417.

(33) Bayer, V.; Podloucky, R.; Franchini, C.; Allegretti, F.; Xu, B.; Parteder, G.; Ramsey, M. G.; Surnev, S.; Netzer, F. P. Formation of $Mn_3O_4(0\ 0\ 1)$ on $MnO(0\ 0\ 1)$: Surface and Interface Structural Stability. *Phys. Rev. B* **2007**, *76*, 165428(1–10).

(34) Liu, Y.; Cen, W.; Wu, Z.; Weng, X.; Wang, H. SO_2 Poisoning Structures and the Effects on Pure and Mn Doped CeO_2: A First Principles Investigation. *J. Phys. Chem. C* **2012**, *116*, 22930–22937.

(35) Shi, L.; Chu, W.; Qu, F.; Hu, J.; Li, M. Catalytic Performance for Methane Combustion of Supported Mn-Ce Mixed Oxides. J. *Rare Earths* **2008**, *26*, 836–840.

(36) Qi, G.; Yang, R. T.; Chang, R. MnOx-CeO_2 Mixed Oxides Prepared by Co-Precipitation for Selective Catalytic Reduction of NO with NH_3 at Low Temperatures. *Appl. Catal., B* **2004**, *51*, 93–106.

(37) Yang, Z.; Woo, T. K.; Baudin, M.; Hermansson, K. Atomic and Electronic Structure of Unreduced and Reduced CeO_2 Surfaces: A First-Principles Study. *J. Chem. Phys.* **2004**, *120*, 7741(1–9).

(38) Arena, F.; Trunfio, G.; Fazio, B.; Negro, J.; Spadaro, L. Nanosize Effects, Physicochemical Properties, and Catalytic Oxidation Pattern of the Redox-Precipitated MnCeO$_x$ System. *J. Phys. Chem. C* **2009**, *113*, 2822–2829.

(39) Chen, Y.; Hu, P.; Lee, M.; Wang, H. Au on (1 1 1) and (1 1 0) Surfaces of CeO_2: a Density-Functional Theory Study. *Surf. Sci.* **2008**, *602*, 1736–1741.

(40) Peng, Y.; Liu, Z.; Niu, X.; Zhou, L.; Fu, C.; Zhang, H.; Li, J.; Han, W. Manganese Doped CeO_2-WO_3 Catalysts for the Selective Catalytic Reduction of NO_x with NH_3: An Experimental and Theoretical Study. *Catal. Commun.* **2012**, *19*, 127–131.

(41) Kotomin, E. A.; Evarestov, R. A.; Mastrikov, Yu. A.; Maier, J. DFT Plane Wave Calculations of the Atomic and Electronic Structure of $LaMnO_3(0\ 0\ 1)$ Surface. *Phys. Chem. Chem. Phys.* **2005**, *7*, 2346–2350.

(42) Piskunov, S.; Heifets, E.; Jacob, T.; Kotomin, E.; Ellis, D.; Spohr, E. Electronic Structure and Thermodynamic Stability of $LaMnO_3$ and $La_{1-x}Sr_xMnO_3(0\ 0\ 1)$ Surfaces: Ab Initio Calculations. *Phys. Rev. B* **2008**, *78*, 121406(1–4).

(43) Wörz, A.; Heiz, U.; Cinquini, F.; Pacchioni, G. Charging of Au Atoms on TiO_2 Thin Films from CO Vibrational Spectroscopy and DFT Calculations. *J. Phys. Chem. B* **2005**, *109*, 18418–18426.

(44) Claeyssens, F.; Freeman, C. L.; Allan, N. L.; Sun, Y.; Ashfolda, M. N. R.; Harding, J. H. Growth of ZnO Thin Films - Experiment and Theory. *J. Mater. Chem.* **2005**, *15*, 139–148.

(45) Shannon, R. D. Revised Effective Ionic Radii and Systematic Studies of Interatomic Distances in Halides and Chalcogenides. *Acta Cryst. A* **1976**, *32*, 751–767.

(46) Henkelman, G.; Arnaldsson, A.; Jónsson, H. A Fast and Robust Algorithm for Bader Decomposition of Charge Density. *Comput. Mater. Sci.* **2006**, *36*, 354–360.

(47) Hwang, B. J.; Tsai, Y. W.; Carlier, D.; Ceder, G. A Combined Computational/Experimental Study on $LiNi_{1/3}Co_{1/3}Mn_{1/3}O_2$. *Chem. Mater.* **2003**, *15*, 3676–3686.

(48) Murugan, B.; Ramaswamy, A. V. Chemical States and Redox Properties of Mn/CeO_2-TiO_2 Nanocomposites Prepared by Solution Combustion Route. *J. Phys. Chem. C* **2008**, *112*, 20429–20442.

(49) García Pintos, D.; Juan, A.; Irigoyen, B. Oxygen Vacancy Formation on the $Ni/Ce_{0.75}Zr_{0.25}O_2(111)$ Surface. A DFT+U study. *Int. J. Hydrogen Energy* **2012**, *37*, 14937–14944.

(50) Chang, R. *Chemistry*, 10th ed.; McGraw-Hill: New York, 2010.